Progress In Electromagnetics Research, Vol. 167, 31–39, 2020

One-Antenna Radiation Pattern Measurement of On-Wafer Antennas in Probe Station Environment

Jianfang Zheng*, Juha Ala-Laurinaho, Zachary D. Taylor, and Antti V. Räisänen

Abstract—We propose and demonstrate the use of radiation pattern measurement method for on-wafer antennas for the first time that is capable of in-depth antenna characterization with limited equipment. This one-antenna method extracts gain without the need for a second antenna in the on-wafer probe station environment. A combination of reference reflector translation and rotation allows radiation pattern sampling at multiple angles enabling characterization over the relevant solid angle. Several microstrip patch antennas with varying beam directions (0°, 20°, and 30°) were measured with the proposed method over 120° in the H-plane with good agreement between simulation and experiment. The method offers a cost-effective and time-efficient solution for probe-fed, on-wafer antenna radiation performance characterization.

1. INTRODUCTION

Millimeter-wave (mm-wave) technologies have been extensively developed for various applications, such as broadband high-data-rate wireless communications and automotive radar [1–4]. In these applications, the antenna is typically integrated with electronics using coplanar waveguide or microstrip feed lines. However, especially in the product development phase, the antenna must be characterized separately. At mm-wave frequencies, it is difficult to interface antennas with a coaxial plug or a waveguide connector since their dimensions are comparable with, or even smaller than, the size of the connectors. Therefore, RF probing is a more common way to feed the antenna under test (AUT) in the mm-wave frequency range.

The radiation pattern measurement of probe-fed antennas was reported in [5], in which an open-ended waveguide was moved along an arc in the far-field of the AUT using a rotator and a Plexiglas arm. Similar measurement setups were built for the probe-fed antennas in the frequency range from 2 GHz to 325 GHz [6–12]. In these works, a robotic arm or similar mechanical assemblies were used to move a second antenna in the AUT far-field to measure the radiation pattern. In [7], the AUT was placed on a small custom-designed sample holder instead of the probe station, which reduces the interference between the AUT and metallic chuck. In [9], instead of a coaxial cable, a rotation arm made of WR-15 waveguide was used to reduce the transmission loss. In [10], the realized gain and axial ratio are quantified, in addition to the AUT radiation pattern.

Another type of radiation pattern measurement in the probe station environment is the planar near-field measurement. A 24-GHz horn antenna was employed as a near-field measurement probe and scanned in two dimensions above the AUT [13]. In [14], an open-ended waveguide probe was proposed to be used to scan the near-field of AUTs up to 325 GHz.

The setup in [15] determines the radiation pattern and gain at 240 GHz from the near-field data. In addition, the effect of probe scattering on the mm-wave antenna measurement accuracy have been studied in [16–18].

Received 18 December 2019, Accepted 8 February 2020, Scheduled 15 March 2020

* Corresponding author: Jianfang Zheng (jianfang.zheng@aalto.fi).

The authors are with the Department of Electronics and Nanoengineering and MilliLab, School of Electrical Engineering, Aalto University, Espoo, AALTO-00076, Finland.

In the aforementioned references, the probe-fed antenna radiation pattern measurement systems all require at least two antennas (AUT and a second antenna). However, there is another easier way to measure the AUT radiation pattern, namely, one-antenna measurement method. In this method, only the AUT and a reflector are needed, and the radiation performance (gain and radiation pattern) can be found from the reflection coefficients. In [19], the antenna radiation pattern was retrieved from reflection coefficients when a reflective load (metal strip) was translated in front of the antenna aperture. From the reflection coefficients the antenna aperture field distribution can be retrieved, and finally the radiation pattern is found through a direct calculation from the equivalent source current.

In [20] and [21], we reported a one-antenna gain measurement method. With the implementation of Fast Fourier Transform (FFT) and time gating, the multiple reflections can be filtered out and then obtain an accurate gain result. However, in that work only the gain values at broadside direction were measured. One-antenna gain method has been applied for radiation pattern measurement in [22] but only for high-gain antennas.

In this paper, we extend the study of [21] by adding a rotator to measure the AUT gain at different angles and determine the antenna radiation pattern for the first time in on-wafer probe station environment. Section 2 introduces the one-antenna gain and radiation pattern measurement method. The design of the AUTs used in this work is presented in Section 3. Finally, the measurement setup is described and the proposed method is demonstrated with different AUTs in Section 4.

2. METHOD

2.1. Gain Measurement

When the AUT radiates towards a sufficiently large, flat perfect electric conductor (PEC) reflector, it serves as the transmitting as well as the receiving antenna. Moreover, if the reflector is positioned in the AUT far-field range, then by applying image theory, Friis' formula can be applied to the AUT and its image (Figure 1).

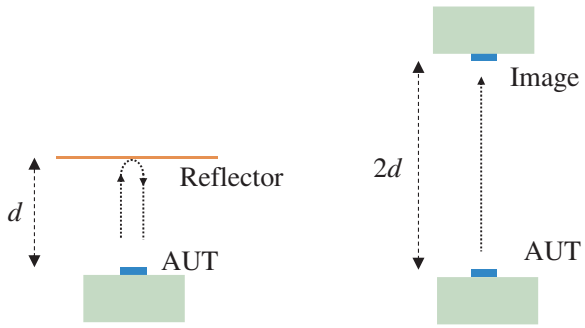

Figure 1. The one-antenna gain measurement method scheme with image theory.

It was reported in [21] that the change in the reflection coefficient S_{11} of the antenna due to the presence of the reflector is:

$$|S_{11\text{dif}}| = \frac{G\lambda}{8\pi d} \tag{1}$$

where λ is the free space wavelength, and d is the distance between AUT and reflector. $S_{11\text{dif}}$ is the difference in S_{11} measured in the presence and absence of the reflector. Eq. (1) can be rewritten as:

$$G = |S_{11\text{dif}}| \cdot \frac{8\pi}{\lambda} \cdot d \tag{2}$$

In principle, the AUT gain is obtained by a single measurement where the reflector is placed at some arbitrary far-field distance. However, the extracted gain is dependent on the distance due to the edge diffraction arising from the limited reflector size [21]. To account measurement system induced

gain variation, the reflector is translated over some range in the reflector broadside direction, and the average of the corresponding gains is defined as the final gain:

$$\bar{G} = \frac{1}{N}\sum_{n=1}^{N} G_n \tag{3}$$

where N denotes the number of reflector locations during the sweep, and G_n is the n^{th} gain value calculated when the reflector is at the n^{th} position in Eq. (2).

As in [21], during the post processing, it is necessary to apply FFT techniques for the frequency domain reflection coefficient at each reflector position to filter out multiple reflections between the reflector and the wafer surface that cannot be covered with absorbers and other possible reflections from the environment. Thus, the measurement accuracy of each G_n is improved.

2.2. Radiation Pattern Measurement

The idea of measuring antenna radiation pattern by the one-antenna gain measurement method is to measure the gain at desired angles, i.e., repeating the gain measurement process described in the previous section at different angles. As shown in Figure 2, the reflector is translated along the θ_1 direction at different positions d_{11}, d_{12}, d_{13}, ..., d_{1N}, S_{11} is measured at each position, and the gain at θ_1 direction can be determined. Similarly, when rotating the reflector to θ_q direction and moving it at distances d_{q1}, d_{q2}, d_{q3}, ..., d_{qN}, the gain value at θ_q direction can be found. Here, $q = 1, \ldots, Q$, where Q is the number of the angle points, and $n = 1, \ldots, N$, where N is the number of the distances. By repeating the process at desired directions, the full radiation pattern is determined.

Compared with the one dimensional (linear) movement in [21], we add a rotator to enable the angular sampling. Detailed measurement setup is described in Section 4.1.

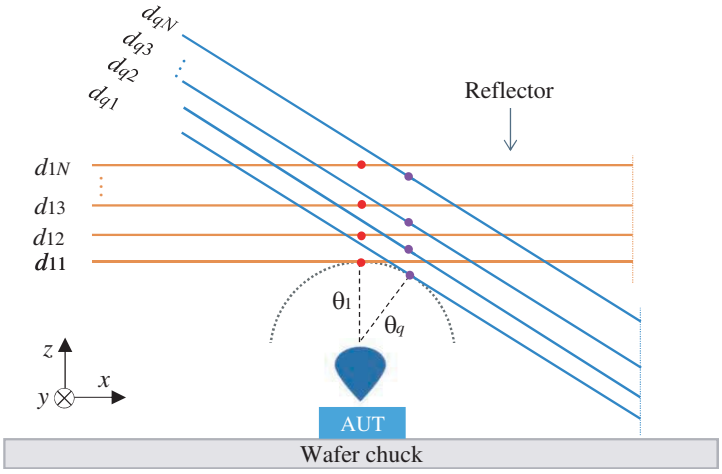

Figure 2. The principle of antenna radiation pattern measurement by measuring the gain values at each angle with a reflector.

3. TEST ANTENNAS

Radiation pattern measurement performance was demonstrated through measurements of microstrip patch antennas operating in the 77-GHz band. Four microstrip patch antennas were designed for this measurement demonstration: 1×1 antenna element and three 1×4 antenna arrays with beams directed at 0°, 20°, and 30°.

The antennas were fabricated by evaporating on a 210-µm thick quartz substrate with a permittivity of $\varepsilon_r = 4.3$, $\tan\delta = 0.003$. Figure 3 shows the design of the antennas (1×1 antenna element and 1×4 antenna array with 0° beam direction and concept of 1×4 array for other directions) with key

dimensional parameters. Other dimensions are: (grounded) coplanar waveguide (CPW) signal line width $w_{\text{signal}} = 90\,\mu\text{m}$; gap between CPW ground and signal line $w_{\text{gap}} = 12\,\mu\text{m}$; 50-Ω, 70-Ω and 100-Ω microstrip line widths are $w_{50\,\Omega} = 0.4\,\text{mm}$, $w_{70\,\Omega} = 0.22\,\text{mm}$ and $w_{100\,\Omega} = 0.15\,\text{mm}$. The 1×4 antenna arrays with 20° and 30° beam directions are implemented by shifting the feeding lines away from the center of the 1×2 power dividers by which phase differences between the elements are created and the desired beam directions are achieved (Figure 3(c)). Table 1 shows the detailed dimensions. During the measurements, the grounded antenna wafer, including large numbers of antennas, is placed on the probe station wafer chuck. The wafer chuck size and computational resource constraints limited simulations to a 70 mm × 80 mm ground plane. Antenna simulation results and corresponding measurements are presented in Section 4.3.

Table 1. Dimensions of antenna arrays in Figure 3(c).

1×4 Antenna Array	$l_{\mathbf{1L}}$ (mm)	$l_{\mathbf{1R}}$ (mm)	$l_{\mathbf{2L}}$ (mm)	$l_{\mathbf{2R}}$ (mm)
Beam towards 20°	0.98	1.92	0.67	1.13
Beam towards 30°	0.85	2.05	0.60	1.20

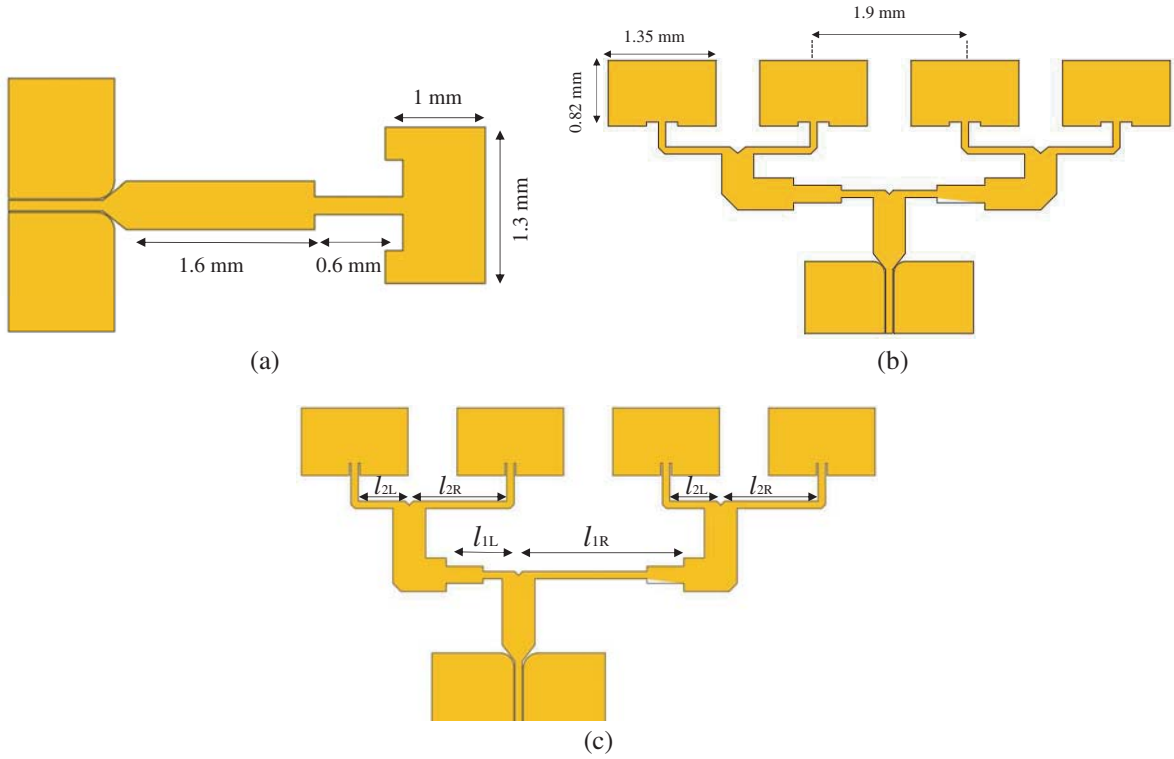

Figure 3. Designed patch antennas with dimensions. (a) 1×1 antenna; (b) 1×4 antenna array with broadside (0°) beam; (c) 1×4 antenna array with other beam directions.

4. MEASUREMENT

4.1. Setup

The measurement setup is shown in Figure 4. Absorber sheets are placed on top of the measurement setup and outside the wafer area. A Standa® translation stage (2.5 µm resolution) and a rotational

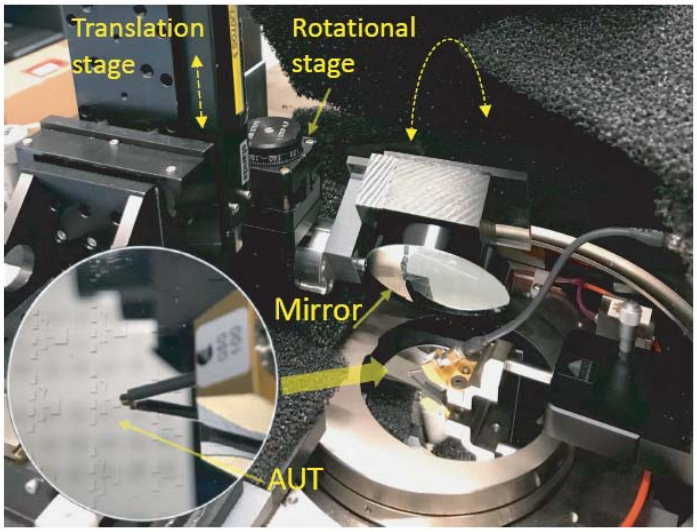

Figure 4. Setup of the antenna radiation pattern measurement.

stage (0.9′ angular resolution) are combined in this measurement and their movements are driven by a motor controller with MATLAB script. After the approximation of the required reflector size by the physical optics method in [21], an aluminum-coated optical mirror with 76 mm diameter is employed as the reflector.

The measurement procedure in brief is: (i) mechanical system alignment and vector network analyzer (VNA) calibration: the alignment is done by using a laser pointer and a gradienter (0.1° resolution) applied in azimuth and inclination; (ii) probing antennas with the aid of the microscope, then lift and remove the microscope for the convenience of translation stage movement; (iii) turn rotator (mirror) and measure S_{11} at each angle; (iv) move translation stage linearly and repeat step (iii); (v) data processing. Figure 5 shows how the measurement proceeds and data are stored. When the translation stage is at a given distance, the VNA sweeps frequencies and records S_{11} data (P frequency points). Then the reflector is rotated over the angular range (Q angle points) and corresponding S_{11} values are stored. Finally the translation stage is moved within the linear moving range (N distance points) and the rotation is repeated to get all measurement data. $S_{11}(f_p, \theta_q, d_{qn})$ denotes the S_{11} value of the p^{th} frequency point when the reflector is at q^{th} angle and n^{th} distance position. Note that d_{qn} is the

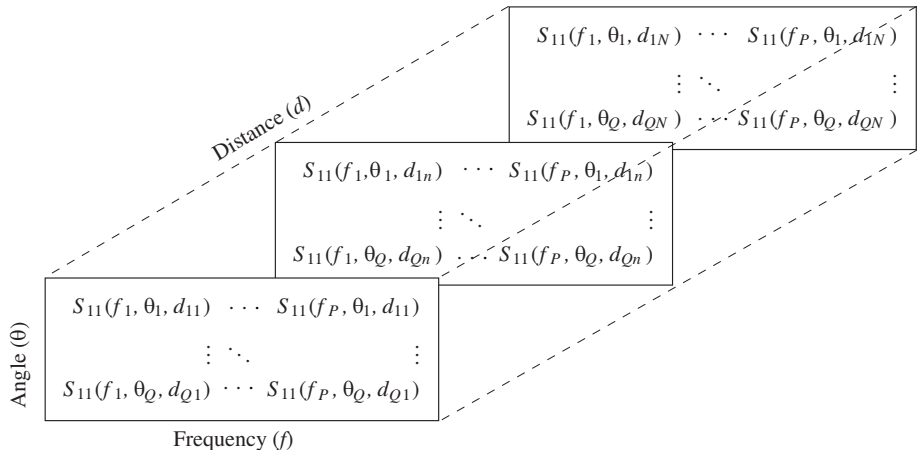

Figure 5. Storage structure of measurement data.

perpendicular distance of the AUT to reflector. The d_{qn} also depends on mirror angle because the AUT is not coincident with the axis of rotation (see Figure 2).

4.2. Reflector

The size of the reflector in the measurement affects the performance of the method: a large reflector brings good accuracy but bulky setup, whereas a compact setup results from a small reflector. There is a trade-off between the measurement accuracy and the system complexity, often parameters such as the largest possible angle.

The physical optics (PO) considering edge diffraction has been applied in the one-antenna simulation, thus, used to select an appropriate reflector [21]. In this work, the effect of the 76-mm diameter aluminum-coated optical mirror is calculated. As a reference, a large enough mirror (diameter 400 mm) is also simulated. The results for patch antenna are shown in Figure 6.

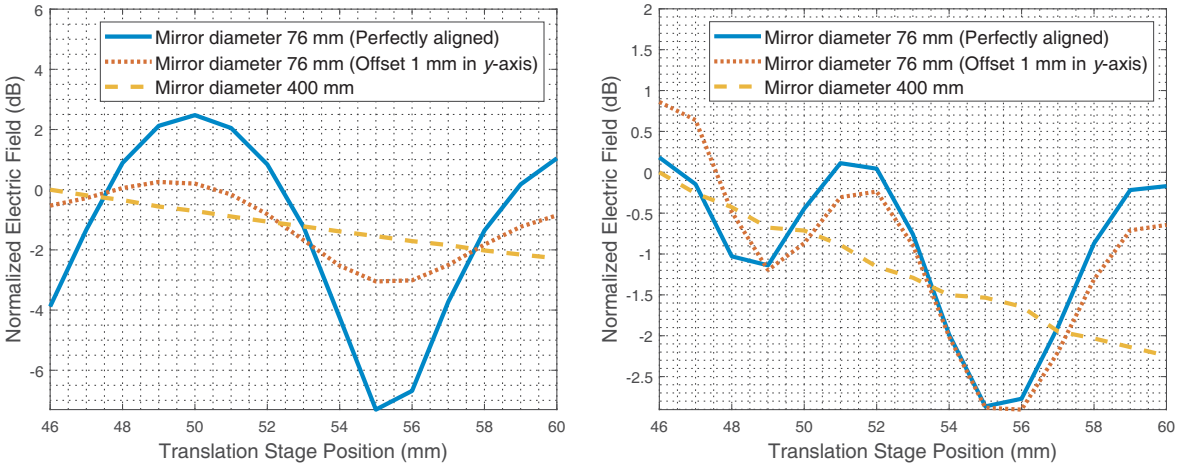

Figure 6. The effect of 76-mm diameter mirror as the reflector, compared with a 400-mm diameter mirror: (a) placed at broadside and (b) rotated at 60°. Calculated by PO [21].

When the reflector is large enough, the reflected electric field decreases smoothly according to $1/d$. For the 76-mm diameter mirror, the electric field has some ripples over distance, which is caused by the mirror edge diffraction. Perfect alignment has the worst ripple level because the mirror edge diffraction superposes from all sides with the same phase. However, a small offset breaks the phase symmetry reducing the diffraction effect. After applying averaging as in Equation (3), the gain value differences by the two mirrors (76-mm vs 400-mm) are 0.71 dB and 0.35 dB at broadside and 60° directions, respectively, and 0.1 dB and 0.3 dB after applying a 1-mm offset, which is acceptable by normal measurement requirement.

4.3. Results

The antennas are fed by a ground-signal-ground probe (Cascade ACP110-GSG-100). The measured reflection coefficients S_{11} towards free space are shown in Figure 7. They have small frequency shifts compared with the simulated ones, but all have good amplitude levels below −10 dB at 77 GHz.

The gains are calculated using the process presented in Section 2.1. Figure 8 shows the measured gain values of all antennas at their designed beam directions in the H-plane. The measured gain curve shapes agree well with simulations, but the measured gain values have frequency shifts similar to those in the measured S_{11} parameters.

As described in Section 2, one-antenna radiation pattern measurements require two degrees of freedom: reflector location and rotational orientation. Due to the obstacle of feeding cable and probe,

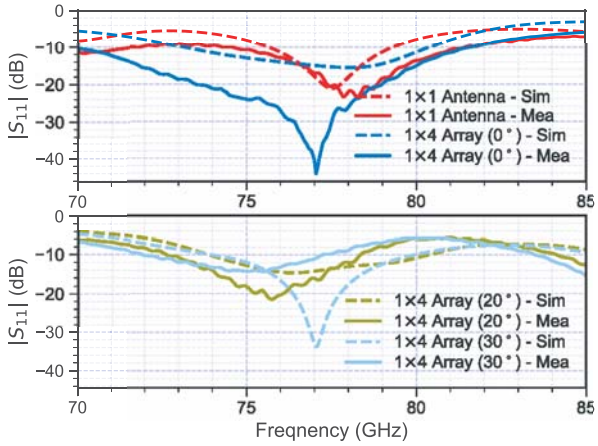

Figure 7. Simulated and measured S_{11} of antennas.

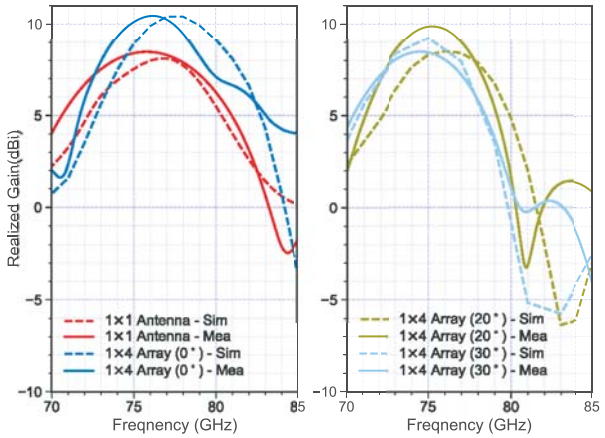

Figure 8. Simulated and measured realized gains of antennas at their own main beam directions (H-plane cut).

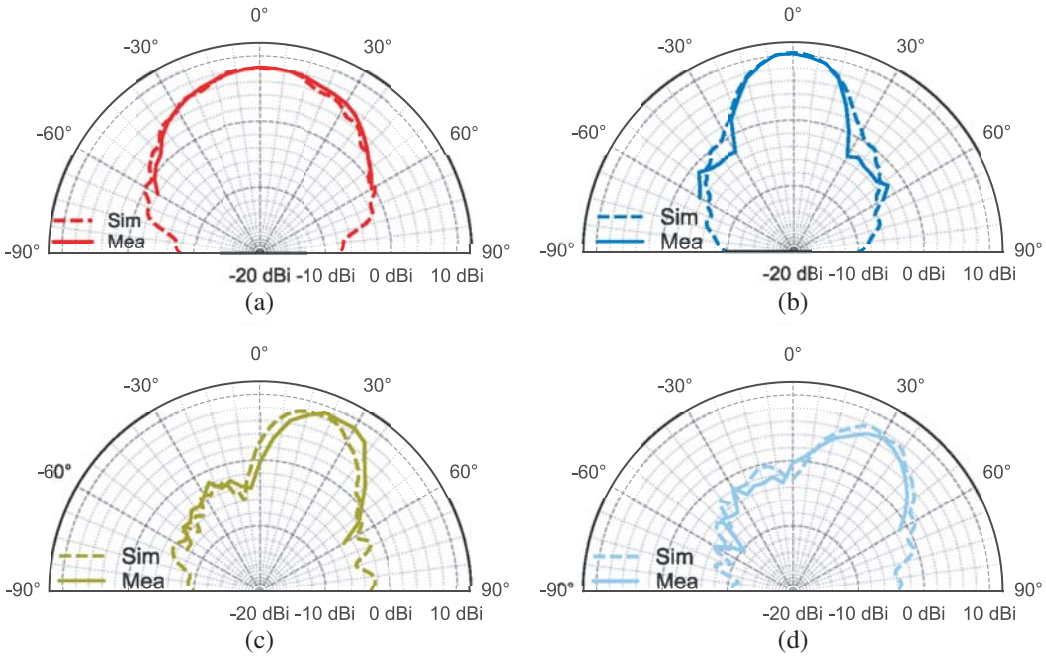

Figure 9. Simulated and measured antenna H-plane radiation patterns (realized gain) at 77 GHz: (a) 1×1 antenna element; (b) 1×4 antenna array with broadside (0°) beam; (c)–(d) 1×4 antenna arrays with 20° and 30° beam directions, respectively.

the reflector cannot rotate along the whole upper half of the E-plane. Therefore, in this measurement we only measured the radiation pattern in the H-plane. Further, these practical constraints limited rotation to ±60° (sampled in steps of 5°) and translation from 46 mm to 60 mm (steps of 1 mm). To increase the measuring range, custom-designed sample holder like in [7] could be used to make the mirror rotating over the upper half H-plane (−90° to 90°).

The measured realized gain radiation patterns are plotted in Figure 9. It is clear that almost all antennas have radiation towards their designed beam directions, and have excellent agreements between the corresponding simulated and measured results: almost the same realized gain levels and beam patterns. For antennas with 20° and 30° beam directions, the measured radiation patterns have small angular shifts compared with simulations. This is most likely because the fabrication error: as

shown in Table 1, a dimensional difference of a few tens of microns will lead to a beam direction difference of 10°. However, for the broadside antennas, because of the dimensional symmetry, no pattern shifts are observed.

5. CONCLUSION

This paper presents for the first time the application of the one-antenna radiation pattern method for on-wafer antennas in the probe station environment. Unlike traditional on-wafer antenna radiation pattern measurement techniques, this method does not require a second antenna and its associated translation mechanics and flexible transmission lines. Our method employs a reflector with a translation stage to measure the antenna gain and the addition of the rotator enables radiation pattern measurement. Several CPW-fed microstrip patch antennas with different beam patterns were fabricated and measured with this method. The results show excellent agreement between the measurement and simulation in the angular range of $-60°$ to $+60°$ in H-plane.

ACKNOWLEDGMENT

The authors thank Dr. Aleksi Tamminen for the controller script and Dr. Andrey Generalov for the lithography process instruction. The first author thanks the HPY Research Foundation for the financial support.

REFERENCES

1. Huang, K. and Z. Wang, *Millimeter Wave Communication Systems*, Wiley/IEEE Press, New York, 2011.
2. Singh, H., J. Oh, C. Kweon, X. Qin, H. Shao, and C. Ngo, "A 60 GHz wireless network for enabling uncompressed video communication," *IEEE Communication Magazine*, Vol. 46, No. 12, 71–78, 2008.
3. Menzel, W. and A. Moebius, "Antenna concepts for millimeter-wave automotive radar sensors," *Proceedings of the IEEE*, Vol. 100, No. 7, 2372–2379, July 2012.
4. Meinel, H. H., "Evolving automotive radar — From the very beginnings into the future," *8th European Conference on Antennas and Propagation (EuCAP 2014)*, 3107–3114, Hague, Netherlands, 2014.
5. Simons, R. N., "Novel on-wafer radiation pattern measurement technique for MEMS actuator based reconfigurable patch antennas," *NASA STI/Recon Technical Report N*, Vol. 2, October 2002.
6. Zwick, T., C. Baks, U. R. Pfeiffer, D. Liu, and B. P. Gaucher, "Probe based MMW antenna measurement setup," *IEEE Antennas and Propagation Society Symposium*, 747–750, Monterey, CA, USA, 2004.
7. Beer, S. and T. Zwick, "Probe based radiation pattern measurements for highly integrated millimeter-wave antennas," *Proceedings of the Fourth European Conference on Antennas and Propagation*, 1–5, Barcelona, 2010.
8. Gulan, H., S. Beer, S. Diebold, C. Rusch, A. Leuther, I. Kallfas, and T. Zwick, "Probe based antenna measurements up to 325 GHz for upcoming millimeter-wave applications," *2013 International Workshop on Antenna Technology (iWAT)*, 228–231, Karlsruhe, Germany, 2013.
9. Ito, T., Y. Tsutsumi, S. Obayashi, H. Shoki, and T. Morooka, "Radiation pattern measurement system for millimeter-wave antenna fed by contact probe," *2009 European Microwave Conference (EuMC)*, 1543–1546, Rome, Italy, 2009.
10. Titz, D., F. Ferrero, and C. Luxey, "Development of a millimeter-wave measurement setup and dedicated techniques to characterize the matching and radiation performance of probe-fed antennas," *IEEE Antennas and Propagation Magazine*, Vol. 54, No. 4, 188–203, 2012.

11. Caekenberghe, K. V., K. M. Brakora, W. Hong, K. Jumani, D. Liao, M. Rangwala, Y. Wee, X. Zhu, and K. Sarabandi, "A 2–40 GHz probe station based setup for on-wafer antenna measurements," *IEEE Transactions on Antennas and Propagation*, Vol. 56, No. 10, 3241–3247, 2008.
12. Ranvier, S., M. Kyrö, C. Icheln, C. Luxey, R. Staraj, and P. Vainikainen, "Compact 3-D on-wafer radiation pattern measurement system for 60 GHz antennas," *Microwave and Optical Technology Letters*, Vol. 51, No. 2, 319–324, 2009.
13. Shamim, A., L. Roy, N. Fong, and N. G. Tarr, "24 GHz on-chip antennas and balun on bulk Si for air transmission," *IEEE Transactions on Antennas and Propagation*, Vol. 56, No. 2, 303–311, 2008.
14. Klein, B., M. Jenning, P. Seiler, K. Wolf, and D. Plettemeier, "On-chip antenna pattern measurement setup up to 325 GHz," *2014 International Symposium on Antennas and Propagation Conference Proceedings*, 175–176, Kaohsiung, 2014.
15. Jam, A. and K. Sarabandi, "A submillimeter-wave near-field measurement setup for on-wafer pattern and gain characterization of antennas and arrays," *IEEE Transactions on Instrumentation and Measurement*, Vol. 66, No. 4, 802–811, April 2017.
16. Mohammadpour-Aghdam, K., S. Brebels, A. Enayati, R. Faraji-Dana, G. A. E. Vandenbosch, and W. DeRaedt, "RF probe influence study in millimeter-wave antenna pattern measurements," *International Journal of RF and Microwave Computer-Aided Engineering*, Vol. 21, No. 4, 413–420, July 2011.
17. Reniers, A. C. F., A. R. van Dommele, A. B. Smolders, and M. H. A. J. Herben, "The influence of the probe connection on mm-wave antenna measurements," *IEEE Transactions on Antennas and Propagation*, Vol. 63, No. 9, 3819–3825, September 2015.
18. Liu, Q., U. Johannsen, M. C. van Beurden, and A. B. Smolders, "Antenna-on-chip radiation pattern characterization — Analysis of different approaches," *2019 13th European Conference on Antennas and Propagation (EuCAP)*, 1–5, Krakow, Poland, 2019.
19. Du, Z., V. Viikari, J. Ala-Laurinaho, A. Tamminen, and A. V. Räisänen, "Antenna pattern retrieval from reflection coefficient measurement with reflective loads," *Progress In Electromagnetics Research*, Vol. 148, 15–22, 2014.
20. Ala-Laurinaho, J., J. Zheng, and A. V. Räisänen, "One-antenna gain measurement in a probe station," *2018 IEEE Conference on Antenna Measurement and Application (CAMA)*, 1–4, Västerås, 2018.
21. Zheng, J., J. Ala-Laurinaho, and A. V. Räisänen, "On the one-antenna gain measurement method in probe station environment at mm-wave frequencies," *IEEE Transactions on Instrumentation and Measurement*, Vol. 68, No. 11, 4510–4517, November 2019.
22. Bhardwaj, S., N. K. Nahar, and J. L. Volakis, "A cost-effective phaseless pattern measurement method for a CP antenna in a submillimeter-wave band," *IEEE Antennas and Wireless Propagation Letters*, Vol. 16, 1683–1686, 2017.